CONCEPTUALIZATION OF CRACK CLOSURE MECHANISM MAPS

VIKAS KUMAR SAXENA and V.M. RADHAKRISHNAN*
Defence Metallurgical Research Laboratory, Kanchanbagh, Hyderabad-500 058 (India)
** Department of Metallurgical Engineering, Indian Institute of Technology, Madras-600036 (India)*

ABSTRACT

A scheme of crack closure mechanism map has been proposed with a view to predict crack closure mechanisms operative under a given set of loading conditions for any alloy/ microstructure. The domains of various crack closure mechanisms are mapped in K_{max}-ΔK space using boundary equations. The governing boundary equations for each domain are derived based on the conditions under which a given crack closure mechanism dominates. The crack closure mechanism maps are constructed for a variety of materials. It is shown that the dominance of a particular mechanism under a given set of loading conditions is dependent on the deformation behaviour, microstructure, yield strength, fracture toughness, texture and component thickness. Some possible engineering applications of crack closure mechanism maps are also described.

Keywords: Fatigue crack growth, crack closure, safe limit

INTRODUCTION

Fatigue crack growth behaviour of a material is influenced by a number of mechanical, microstructural and environmental factors. Attempts have been made to rationalize the effects of these factors by invoking the crack closure concept, a phenomenon first discovered by Elber (1970). A fatigue crack experiencing tension-tension cyclic loading can fully or partially be closed during a part of the cycle due to various crack closure mechanisms (Suresh, 1991). Recently, crack closure concept has been incorporated in the fracture mechanics based life prediction models to account for stress ratio and load interaction effects. In order to exploit the crack closure concept in life predictions, it is important to know the type of crack closure mechanism operative under a given loading condition. Here, a concept of crack closure mechanism map has been proposed which predicts the type of crack closure mechanism dominant under specific conditions. Based on the scheme evolved, the closure mechanism maps for a variety of materials are constructed using the experimental data reported elsewhere (Saxena, 1994).

BASIC SCHEME OF CRACK CLOSURE MECHANISM MAP

There are mainly five types of crack closure mechanisms, identified as: plasticity-induced crack closure (PICC), roughness-induced crack closure (RICC), oxide-induced crack closure (OICC), fluid-induced crack closure (FICC) and transformation-induced crack closure (TICC). Of these, PICC, OICC and RICC mechanisms have been widely reported to occur in most of the metallic

systems (Liaw, 1988). The fields of PICC, RICC and OICC mechanisms as well as safe (no crack growth) regime are mapped in K_{max}-ΔK space. The two dimensional K_{max}-ΔK space is constructed with maximum stress intensity factor (SIF), K_{max}, as ordinate and the applied SIF range, ΔK as abscissa (Fig.1). The lines of constant stress ratio, R are drawn using the basic equation $K_{max} = \Delta K/(1-R)$. The line corresponding to R=0 divides the map diagonally into two halves at 45° angle, thus representing the two major types of fatigue loading, namely, tension-tension (R>0, i.e., upper region) and tension-compression (R < 0, i.e., lower region). The field boundaries are derived from the equations defining the conditions under which a given mechanism of crack closure operates. Here, the governing boundary conditions of various regimes are outlined only in brief. The detailed derivation is described elsewhere (Saxena and Radhakrishnan, 1996).

Safe Zone

The area OABCDE representing the safe regime is defined by the locus of threshold limit, ΔK_{th} in K_{max}-ΔK space. One such relation is given as:

$$\Delta K_{th} = \Delta K_{th,0}\,(1-R) \quad for\ 0.8 \geq R \geq 0 \tag{1a}$$

where $\Delta K_{th,0}$ is the threshold limit at R=0. The experimental data for a variety of materials indicate that beyond at a critical stress ratio, R^*, the ΔK_{th} remains constant with R. This could be equated to an effective threshold, $\Delta K_{eff,th}$, by the relation:

$$\Delta K_{th} = \Delta K_{eff,th} \quad for\ R \geq 0.8 \tag{1b}$$

This is indicated by a vertical line CD on the map. The value of R^* has been assumed to be 0.8, based on the investigation by Marci (1992). For R<0 i.e., regime OAB, it is difficult to establish such a relation due to lack of experimental data base.

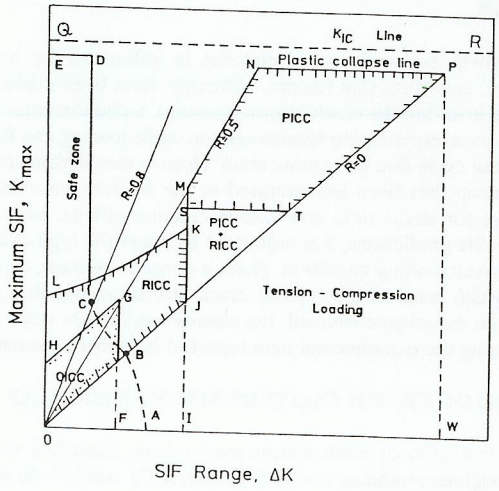

Fig.1 : Schematic of crack closure mechanism map

Oxide-Induced Crack Closure (OICC) Regime

The field equations for OICC regime are derived from the condition that the corrosive deposits exert a mechanical wedging force under cyclic loading when the size of product becomes comparable to crack tip opening displacement (CTOD).

Condition I : The minimum SIF, K_{min}, should be less than the closure SIF, K_{cl}. In other words, the minimum CTOD level, δ_{min}, should be atleast be equal to the product height, t, to make the contact between the fracture surfaces :

$$\delta_{min} \leq t \quad where \quad \delta_{min} = \frac{K_{min}^2}{\sigma_{ys}.E} \tag{2a}$$

On combining, the condition reduces to:

$$K_{max} \leq \Delta K + \sqrt{\sigma_{ys}.E.t} \tag{3b}$$

Condition II : The cyclic CTOD, δ_c, should be less than or equal to oxide product height, t:

$$\delta_c \leq t \quad where \quad \delta_c = 0.5\frac{\Delta K^2}{2\sigma_{ys}.E} \tag{3a}$$

On substituting, condition reduces to :

$$\Delta K \leq 2\sqrt{\sigma_{ys}.E.t} \tag{3b}$$

The OICC regime, represented by the area OFGH, is bound by the Eqns.(2b) and (3b).

Roughness-Induced Crack Closure Regime

The RICC mechanism arises from the premature contact of fracture surface asperities during unloading part of fatigue cycle. The following conditions are required to be satisfied for RICC mechanism to operate.

Condition I: The reversed plastic zone size, r_p^c, should be less than the notational grain size (d). It could be represented as:

$$r_p^c \leq d \quad where \quad r_p^c = 0.033\,(\Delta K/\sigma_{TS})^2 \tag{4a}$$

On combining, the boundary condition reduces to:

$$\Delta K \leq 5.5\ \sigma_{TS}\sqrt{d} \tag{4b}$$

This condition is represented by a vertical line IK on the map.

Condition II: During unloading, the crack surfaces would make contact when the instantaneous CTOD, δ_i, attains a critical value of the order of asperity height, h:

$$\delta_i \leq h \tag{5a}$$

The relation for δ_i is established by extending analytical model, originally developed for plasticity-induced crack closure by Budiansky and Hutchinson (1978). This condition reduces to:

$$K_{max} \leq \frac{\sqrt{\Delta K^2 + 2h\sigma_{ys}E}}{2} \quad (5b)$$

The area OJKL bound by locus of the Eqns. (4b) and (5b) represents RICC regime on the map.

Plasticity-Induced Crack Closure (PICC) Regime

The PICC mechanism arises due to presence of compressive residual stresses caused by strain mismatch at the crack tip during unloading. Based on the mechanism, the following conditions could be formulated mathematically.

Condition I : Crack tip plasticity should exceed the grain size. The governing boundary equation, as derived earlier (Eq.4b), reduces to:

$$\Delta K \geq 5.5\ \sigma_{YS}\sqrt{d} \quad (6a)$$

This condition is represented by line IM on the map.

Condition II: The instantaneous CTOD, δ_i, should be atleast equal to the residual plastic stretch (δ_R) left behind the advancing crack front. This condition is derived based on the model proposed by Budiansky and Hutchinson (1978) as below:

$$K_{max} \leq 1.865\ \Delta K \quad (6b)$$

The line OMN represents this condition.

Condition III: PICC would disappear when the elastic constraints required to confine the residual plastic stretch disappear completely. The condition for plastic collapse, based on specimen size criteria prescribed in ASTM-E647 standard for validity of fatigue crack growth data, is given by the relation:

$$K_{max} \leq 0.5\ \sigma_{ys}\sqrt{\pi(W-a)} \quad for\ CT\ specimen \quad (7a)$$

$$K_{max} \leq 0.9\ \sigma_{ys}\sqrt{\pi a} \quad for\ SENT\ specimen \quad (7b)$$

This condition corresponds to boundary NP on the map. In the case of high strength materials, the condition of plastic collapse would be preceded by catastrophic fracture, defined by fracture toughness,K_{Ic}. This boundary equation:

$$K_{max} \leq K_{Ic} \quad (7c)$$

is indicated by line QR on the map.

Condition IV: The extent of plasticity, hence dominance of PICC mechanism would also be dictated by thickness of the specimen.The specimen thickness criteria, prescribed in ASTM-E399 standard for plane strain condition, appears to be a logical choice in the present analysis. According to this condition, the relation:

$$K_{max} \geq \frac{\sqrt{B\ \sigma_{ys}^2}}{2.5} \quad (8)$$

is indicated by the line ST on the map. The area STPNM represents the PICC regime on the map.

CONSTRUCTION OF CRACK CLOSURE MAPS FOR VARIOUS MATERIALS

The crack closure maps for various materials, namely, Ni-Cr free austenitic steel (Fe-0.4C-17Mn-3Al; solutionized), an AISI-4330 steel (Fe-0.3C-1.4Cr-1.6Ni-0.5Mo-0.1V; quenched and tempered) and an α-β titanium alloy (Ti-6.3Al-3.5Mo-1.9Zr-0.23Si; α-β heat treated) are constructed using the boundary equations (1-8). The three microstructures (designated as T1, T2 and T3) constituting: (i) fully Widmanstatten α phase, (ii) equiaxed primary α phase dispersed in the matrix of transformed β and (iii) equiaxed primary α dispersed in the matrix of metastable β phase were produced mainly to bring out the effect of phase morphology on the various domains of crack closure mechanism map.

Austenitic Steel

The closure map for the austenitic steel is shown in Fig.2. The RICC and PICC regimes are observed to dominate. The OICC field is shown to be absent due to austenitic steels being inheritantly oxidation resistant. Due to lower strength of the material ($\sigma_{ys} \approx 390$ MPa), the PICC regime is well expanded till the point of plastic collapse. The transition (ST line) in the crack closure mechanism from RICC to PICC at $\Delta K \approx 18$ MPa$\sqrt{m}$, as predicted by the map, matches well with the measured crack closure data (Saxena and Radhakrishnan, 1996) in terms of K_{cl}/K_{max} vs ΔK plots. The crack closure mechanisms have been identified from behaviour of crack closure plots, as argued by Allision (1988) and McClung (1990). The fractographs (inset Fig.2) corresponding to the two regimes further provide the evidence to this effect. In PICC regime, the well defined striations are observed. On the other hand, the RICC regime exhibits a structure-sensitive nature of crack growth.

AISI-4330 Steel

The crack closure map for the AISI-4330 steel is shown in Fig.3. In this case, both OICC and RICC are observed to govern the crack growth. The OICC mechanism would operate in low ΔK regime due to presence of a thin oxide layer, assumed to be of the order of 1 μm (Liaw, 1988). The PICC regime is predicted to be absent in this particular steel due to its high strength (σ_{ys} = 1420 MPa) and lower fracture toughness (K_{IC}=60 MPa$\sqrt{m}$). The material would fracture catastrophically before the onset of PICC regime. The closure data as well as fractographic studies confirm these predictions. The fractographic features (inset Fig.3) indicate that the crack growth occurs predominantly by quasi-cleavage at lower as well as higher ΔK levels. The structure-sensitive fractographic features lead to enhanced crack closure by RICC mechanism which remains active even in higher ΔK regime.

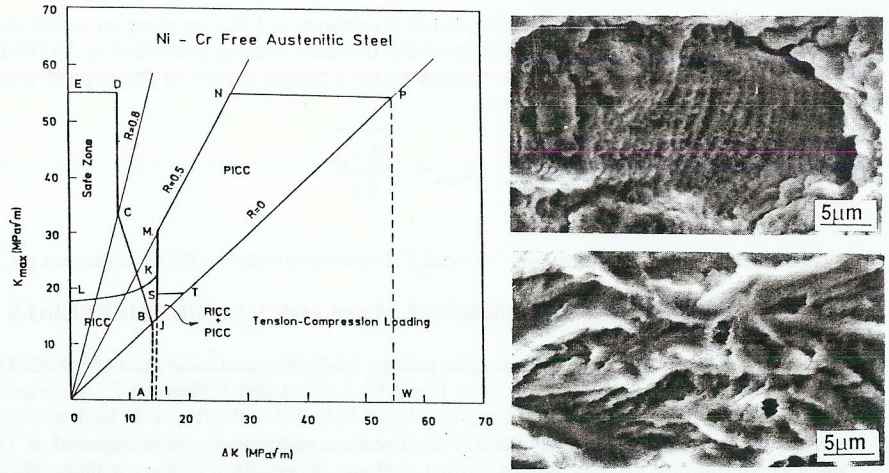

Fig.2 : Crack closure mechanism map of austenitic steel.

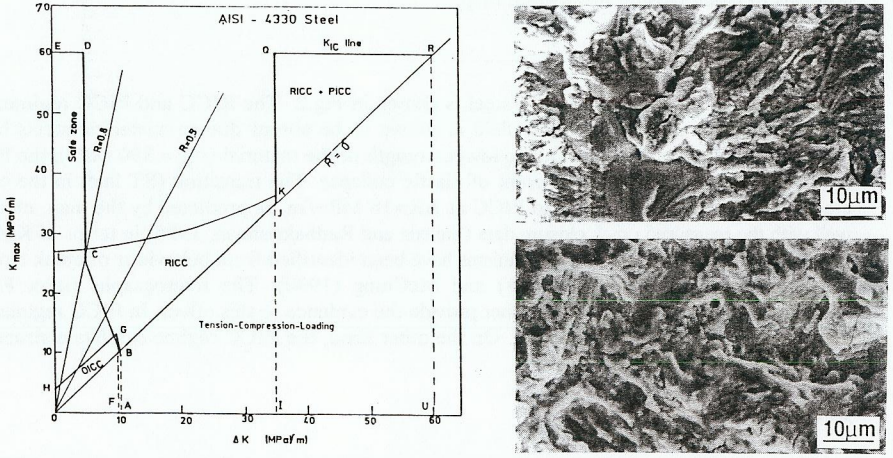

Fig.3 : Crack closure mechanism map of AISI-4330 steel.

α-β Titanium Alloy

The crack closure maps of α-β titanium alloy corresponding to the three microstructural conditions (inset Fig.4), namely, T1, T2 and T3 are shown in Fig.4(a-c). The measured crack closure data, fractographic features and the corresponding crack path profiles (inset Fig.4) has been used to identify the operating crack closure mechanisms. In all the cases, both RICC and PICC mechanisms are operative. The OICC regime is shown to be absent due to higher oxidation resistance of titanium alloys. There is a systematic change in the dominance of various regimes with the microstructure. The RICC mechanism is more dominant in T3 condition as compared to

T1 and T2 cases. It is attributed to presence of large facets introduced by extensive crystallographic cracking of Widmanstatten packets. While in T1 microstructure comprising metastable ß as matrix, the PICC appears to be the primary mechanism controlling the crack growth behaviour till the point of fracture (line RQ). The dominance of PICC in T1 case is attributed to its lower strength (σ_{ys} ≈615 Mpa) as against the T2 and T3 microstructures comprising transformed ß of higher strength (σ_{ys}≈955 MPa). The plasticity in T1 microstructure is further enhanced due to the occurrence of transformation-induced plasticity (TRIP) phenomenon in metastable ß phase during its deformation, as confirmed by transmission electron microscopic studies. It is quite evident on the corresponding fractograph (inset Fig.4a), showing regions of severe plasticity in the form of bands of tearing ridges, joining together and forming serpentine glide-like features.

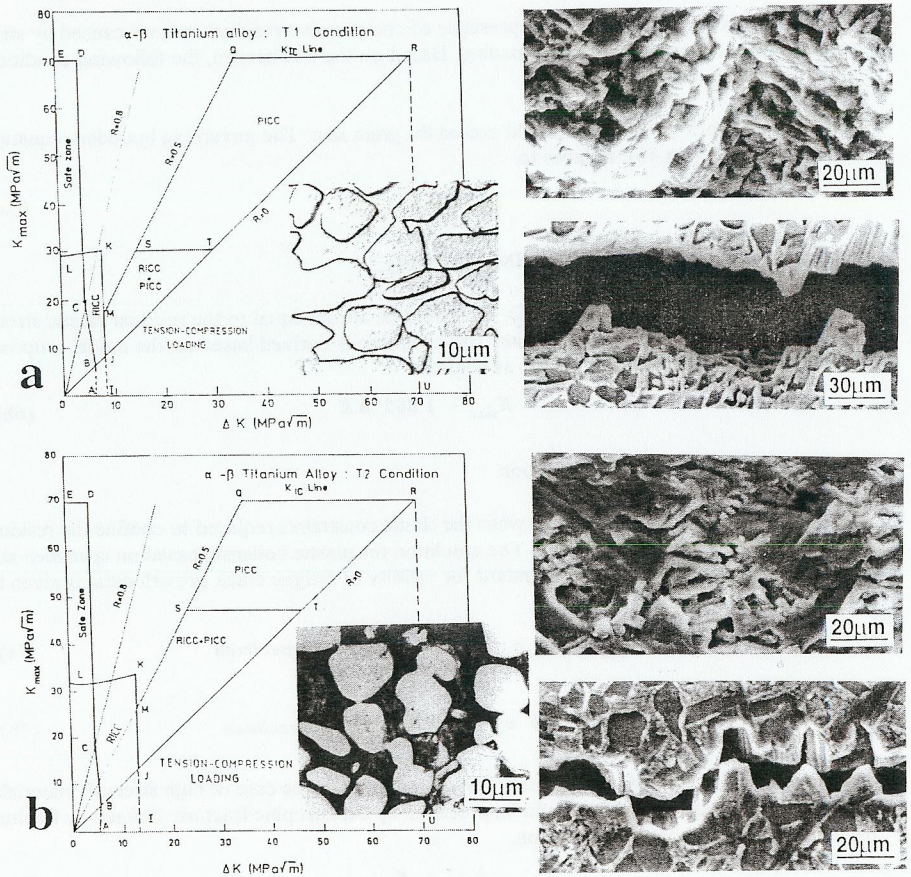

Fig.4: Crack closure mechanism map of titanium alloy under various microstructural conditions : (a) T1, (b) T2 and (c) T3.

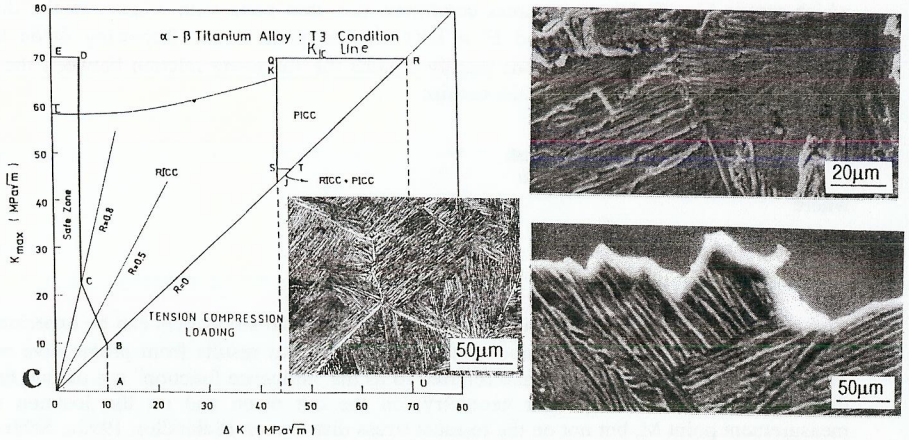

ENGINEERING APPLICATIONS OF CRACK CLOSURE MECHANISM MAPS

The concept of crack closure mechanism map could have significance from the consideration of design based on fatigue crack propagation. The maps could be used in two ways. Firstly, it is possible to develop alloys/microstructures with superior fatigue crack growth resistance. The aim should be to tailor an alloy/microstructure in such a way as to expand the boundaries of various regimes to maximum extent without affecting the toughness. In this regard, the factors such as enhanced planarity of slip, coarse grain, texture, dual phase microstructures and lower yield strength are expected to widen the boudaries. Secondly, from the map, it is possible to predict the type of crack closure mechanism operative under a given set of loading conditions. Once the mechanism is known, the crack closure levels, K_{cl} could be estimated by empirical, analytical or numerical procedures and subsequently, the ΔK_{eff} ($\Delta K_{eff}=K_{max}-K_{cl}$) be determined. This ΔK_{eff} value could be further used to predict crack growth rates in a component by using the modified Paris equation: $da/dN = C(\Delta K_{eff})^m$.

REFERENCES

Allison, J.E. (1988). Measurement of crack closure during fatigue crack growth. *ASTM STP*, **945**, 913-933.

Budiansky, B. and J.W. Hutchinson (1978). Analysis of crack closure in fatigue crack growth. *J. Applied Mech.*, **45**, 267-276.

Elber, W. (1970). Fatigue crack closure under tension. *Engg. Fract. Mech.*, **2**, 37-45.

Liaw, P.K. (1988). Overview of crack closure at near threshold fatigue crack growth levels. *ASTM STP*, **982**, 62-92.

Marci, G. (1992). A fatigue crack growth threshold. *Engg. Fract. Mech.*, **41**, 367-385.

McClung R.C. (1990). The influence of applied stress, crack length and stress intensity factor on crack closure. *Metall. Trans.*, **22A**, 1559-1570.

Saxena Vikas K. (1994). *Mechanical and metallurgical aspects of fatigue crack closure'*, Ph.D., Dissertation, Indian Institute of Technology, Madras (India).

Saxena, Vikas K. and V.M. Radhakrishnan (1996). Development of crack closure maps- Part I: Basic concepts and boundary equations; Part II: Construction of maps of various materials. Communicated to *Acta Metall. Mater.*

Suresh, S. (1991). In: *Fatigue of Materials*, Chap 7, 222-253. Cambridge University Press, Cambridge.